



# **Geophysical Research Letters**



# RESEARCH LETTER

10.1029/2021GL095204

### **Key Points:**

- The second leading mode of tropical Pacific precipitation variability shows a meridional dipole pattern called the Pacific precipitation dipole mode (PPDM)
- PPDM amplifies and reverses its sign between developing and decay phases of extreme El Niño, indicating a nonlinear feature of ENSO
- Coupling between sea surface temperature anomalies and seasonal cycle in the eastern Pacific excites PPDM, which is a manifestation of ENSO combination mode

#### **Supporting Information:**

Supporting Information may be found in the online version of this article.

#### Correspondence to:

M. Watanabe, hiro@aori.u-tokyo.ac.jp

# Citation:

Fukuda, Y., Watanabe, M., & Jin, F.-F. (2021). Mode of precipitation variability generated by coupling of ENSO with seasonal cycle in the tropical Pacific. *Geophysical Research Letters*, 48, e2021GL095204. https://doi.org/10.1029/2021GL095204

Received 2 APR 2021 Accepted 27 JUL 2021

© 2021. The Authors.

This is an open access article under the terms of the Creative Commons Attribution-NonCommercial License, which permits use, distribution and reproduction in any medium, provided the original work is properly cited and is not used for commercial purposes.

# Mode of Precipitation Variability Generated by Coupling of ENSO With Seasonal Cycle in the Tropical Pacific

Yoshihiro Fukuda<sup>1</sup>, Masahiro Watanabe<sup>1</sup>, and Fei-Fei Jin<sup>2</sup>

<sup>1</sup>Atmosphere and Ocean Research Institute, The University of Tokyo, Kashiwa, Japan, <sup>2</sup>Department of Atmospheric Sciences, School of Ocean and Earth Science and Technology, University of Hawai'i at Mānoa, Honolulu, HI, USA

**Abstract** Tropical precipitation anomalies show very different patterns over the central-eastern equatorial Pacific between the developing and decay phases of extreme El Niño despite similar patterns of sea surface temperature (SST) anomalies. Using observational data and atmospheric simulations for 1979–2018, we identified a meridional dipole mode of tropical precipitation variability, called the Pacific precipitation dipole mode (PPDM), which is critical for seasonally varying rainfall patterns related to extreme El Niño. We examined the mechanism of PPDM using a numerical model and found that the seasonal shift of the warm SST band in the eastern equatorial Pacific, when coupled with extreme SST anomalies, causes phase reversal of the PPDM. The PPDM can be regarded as a different manifestation of the El Niño/Southern Oscillation combination mode, as revealed by the surface wind anomalies, which also explains the distinct impact of extreme El Niño events over East Asia.

Plain Language Summary The rainfall patterns over the tropical Pacific are altered by the underling sea surface temperatures (SSTs). The patterns of rainfall anomalies, that is, deviation from climatological mean states, vary between the developing and decay seasons of extreme El Niño, despite similarity in patterns of SST anomalies. Using observational data and atmospheric simulations driven by observed SST for 1979–2018, we identified a meridional dipole mode of tropical rainfall variability that was asymmetric about the equator, called the Pacific precipitation dipole mode (PPDM). PPDM changes the polarity between autumn and spring, before and after the peak of extreme El Niño, and therefore is critical for seasonally varying rainfall patterns related to extreme El Niño. We examined factors that control the polarity of the PPDM by using a mechanistic model of the atmosphere and found that a coupling between SST anomalies associated with extreme El Niño and the seasonal cycle of the warm SST band in the eastern Pacific, migrating between the two hemispheres in a year, causes PPDM to change polarity between autumn and spring. The excitation of PPDM explains a distinct climatic impact over East Asia during extreme El Niño and also a feedback to extreme El Niño.

# 1. Introduction

El Niño/Southern Oscillation (ENSO) is the most dominant mode of coupled atmosphere-ocean variability in the present climate (Neelin et al., 1998; Wallace et al., 1998). It is characterized by sea surface temperature (SST) anomalies in the central-eastern equatorial Pacific. The positive phase with the warm SST anomaly is called El Niño and the negative phase is called La Niña. ENSO occurs quasi-periodically every 3–7 years, and both atmosphere and ocean show large deviations from their climatological mean states once either phase of ENSO appears.

Several studies have shown that ENSO is not independent of the background seasonal cycle in the tropical Pacific (Jin et al., 1994; Stein et al., 2014; Tziperman et al., 1994; Zebiak et al., 1987). The observed ENSO time evolution is locked to the calendar seasons, developing during boreal summer and autumn, reaching its mature phase in boreal winter, and then decaying during the following spring. This cycle results from a coupling with the seasonal cycle that modulates feedback processes for ENSO growth and decay. The above-mentioned modeling and theoretical works have demonstrated that this ENSO phase locking is primarily attributed to the seasonal march of the equatorial subsurface ocean state, which favors the growth of ENSO in summer.

Recent research has suggested that the coupling of the seasonal cycle and ENSO gives rise to the combination mode (C-mode) that helps in rapid termination of strong ENSO events (Stuecker, Jin, &

FUKUDA ET AL. 1 of 10



Timmermann, 2015; Stuecker, Jin, Timmermann, & Megregon, 2015; Stuecker et al., 2013). Some studies have focused on the seasonal migration of westerly wind anomalies over the western equatorial Pacific, while others have focused on precipitation variability (McGregor et al., 2012; Spencer, 2004; Stuecker, Jin, & Timmermann, 2015; Stuecker, Jin, Timmermann, & Megregon, 2015; Stuecker et al., 2013; Xie et al., 2018). While the essential mechanism of the C-mode was shown, the comprehensive understanding has not yet been achieved.

During El Niño, warm SSTs in the western equatorial Pacific extend to the east, and the rainfall distributions, anchored by the warm SST regions, change in a way that precipitation increases over the central equatorial Pacific and decreases over the maritime continent. Diabatic heating anomalies associated with anomalous precipitation drive global ENSO teleconnection by exciting the quasi-stationary Rossby waves in the troposphere (Horel & Wallace, 1981; Hoskins & Karoly, 1981). Previous research has shown that ENSO teleconnection patterns vary among individual events (Chiodi & Harrison, 2013; Okumura, 2019; Yu et al., 2012; Yuan & Yang, 2012), and the difference in teleconnections can be attributed to differences in the tropical rainfall anomaly pattern caused by ENSO SST anomalies (Choi et al., 2013, 2015; Johnson & Kosaka, 2016). In particular, extreme El Niño is known to accompany the rainfall anomaly pattern that differs from other ENSO events (Borlace et al., 2014; Cai et al., 2012). However, the mechanisms that generate these precipitation anomaly patterns observed only during extreme El Niño events are yet to be investigated in detail.

We aim at understanding the mechanisms of precipitation variability associated with ENSO, with particular attention to anomalous states during extreme El Niño. In Section 2, we describe the data sets that were analyzed and the numerical model utilized in this study. In Section 3, the dominant mode of precipitation variability over the tropical Pacific and its possible mechanisms are explained. Section 4 gives a summary and discussion.

# 2. Data and Model

# 2.1. Observational and Reanalysis Data

We used monthly SST data from the Centennial In Situ Observation-Based Estimates of the Variability of SST and Marine Meteorological Variables (COBE-SST2) for 1979–2018 on a  $1^{\circ} \times 1^{\circ}$  horizontal grid (Hirahara et al., 2014). The data before 1979 are available but were not used for the analysis to match the availability of other data sets. We also used monthly precipitation data compiled at the Global Precipitation Climatology Project (GPCP) for 1979–2018 (Adler et al., 2003) with a horizontal resolution of  $2.5^{\circ} \times 2.5^{\circ}$ . Other atmospheric variables, such as temperature, horizontal winds, stream function, and sea level pressure, were derived from the Japanese 55-year Reanalysis (JRA55) data set, with a horizontal resolution of  $1.25^{\circ} \times 1.25^{\circ}$  (Kobayashi et al., 2015). The data period spanned 40 years (1979–2018), similar to the SST and precipitation data.

For all the observational and reanalysis data, we first calculated anomalies by subtracting the monthly climatology defined by the 30-year mean for the 1981–2010 period. All anomalies were then detrended for the entire period. To identify ENSO events, the Niño3.4 index (normalized SST anomaly averaged over  $5^{\circ}$ S– $5^{\circ}$ N and  $120^{\circ}$ – $170^{\circ}$ W) was used. We defined an El Niño year as the year when the Niño3.4 index, averaged from September to February of the following year, exceeded one standard deviation (SD) and defined a La Niña year as the year when the index was below -1 SD. For the 40-year period from 1979 to 2018, we detected nine El Niño (1982/83, 1986/87, 1987/88, 1991/92, 1994/95, 1997/98, 2002/03, 2009/10, and 2015/16) and eight La Nina (1984/85, 1988/89, 1995/96, 1998/99, 1999/2000, 2007/08, 2010/11, and 2011/12) events. Three out of the nine El Niño events (1982/83, 1997/98, and 2015/16) are known to be very strong and are referred to as extreme El Niño events, whereas the other six events are called moderate El Niño events.

# 2.2. Database for Policy Decision Making for Future Climate Change (d4PDF)

The sample size of the observed El Niño and La Niña events may not be sufficient, making it difficult to obtain statistically robust estimates of precipitation variability. To overcome this shortcoming, we used a large ensemble of global atmospheric simulations forced by observed SST, sea-ice concentration, and radiative

FUKUDA ET AL. 2 of 10



forcing for 1979–2017 from the database for Policy Decision making for Future climate change (d4PDF) (Mizuta et al., 2017). This database consists of a set of 100-member simulations using the MRI-AGCM3.2 with a 60 km horizontal resolution and 64 vertical levels. We used monthly data of precipitation and atmospheric variables and applied the same procedure to the observed data before the analysis. While the ensemble was generated by adding tiny perturbations to SSTs within observational uncertainty, we applied the same definition for El Niño and La Niña years as in the observational analysis. Because of the large ensemble size, we used 300, 600, and 800 samples for extreme El Niño, moderate El Niño, and La Niña events, respectively. The MRI-AGCM3.2 shows a good performance of the tropical circulation and precipitation variability, as described in Mizuta et al. (2017) and references therein.

#### 2.3. Moist Linear Baroclinic Model

To understand the mechanisms of precipitation variability, we used a moist linear baroclinic model (mLBM), which is based on primitive equations linearized about a basic state (Watanabe & Jin, 2003). This model solves the steady perturbation of not only dry atmospheric variables (vorticity, divergence, temperature, and logarithm of surface pressure) but also specific humidity and precipitation, the latter obtained by using a linearized convection scheme incorporated into the model. The steady solution is then computed to an imposed pattern of SST anomalies, unlike diabatic heating in a dry model, under prescribed mean states of the atmosphere and SST. The mLBM has the horizontal resolution of T42 (128  $\times$  64 grid points) and 20 vertical levels. The observed seasonal mean climatology of the atmosphere and SST was used to define the basic states of the mLBM. We integrated the model for 30 days to obtain quasi-steady atmospheric responses to imposed SST anomalies and averaged the last 10 days to obtain the steady state response.

#### 3. Results

#### 3.1. Dominant Modes of Precipitation Variability in the Tropical Pacific

Focusing on the anomalous precipitating variability associated with extreme El Niño events defined in Section 2.1, a composite analysis was conducted. Figure 1 shows composites of SST and precipitation anomalies averaged during August-September-October before the mature phase (denoted as ASO(0)) and February-March-April after the peak phase (FMA(1)) of extreme El Niño. SST anomaly patterns in these two seasons resemble each other, with the maximum of approximately 3 K off the coast of Peru (Figures 1a and 1b). Nevertheless, precipitation anomaly patterns are distinct in the two seasons: positive anomalies are located over the central-eastern Pacific in ASO(0), but they are shifted toward the south of the equator in FMA(1) (Figures 1c and 1d). Negative precipitation anomalies are commonly found over the maritime continent but extend eastward over the northern off-equator in FMA(1). The seasonally varying precipitation anomalies are significant over the eastern equatorial Pacific, where composite positive anomalies shifted southward with time (Figure S1). Such differences in precipitation anomalies between the two seasons, as seen during extreme El Niño, are not identified in moderate El Niño years (Figure S2).

To identify the dominant patterns of precipitation variability over the tropical Pacific, we performed an empirical orthogonal function (EOF) analysis to monthly observed precipitation anomalies over the central-eastern equatorial Pacific (15°S–15°N and 180°–80°W, red box in Figure 2a). Figure 2 shows the precipitation anomaly patterns regressed on the corresponding principal component (PC) time series. The two EOFs, accounting for 23.1% and 11.8% of the total variance, respectively, are both large scale and spatially orthogonal to each other by definition. The EOF1 represents a mode of quasi-symmetric precipitation variability about the equator but with a zonal contrast between the central and the western Pacific basins (Figure 2a). This pattern is similar to the well-known anomalous precipitation distribution associated with the peak phase of El Niño (Hoerling et al., 2001; Wallace et al., 1998).

The EOF2 represents a meridional dipole mode with opposite signs of anomalies over the northern and southern off-equatorial Pacific (Figure 2b). Unlike EOF1, there is no large anomalies over the western Pacific. One may suspect that this pattern results from an orthogonal constraint of the EOF analysis and therefore a statistical artifact, but the precipitation anomalies over the two centers of action (northern and southern off-equatorial strips) are indeed coherent, with a significant negative correlation (r = -0.45, see Figure S3), suggesting that the EOF2 pattern is not an artifact but has a physical origin.

FUKUDA ET AL. 3 of 10

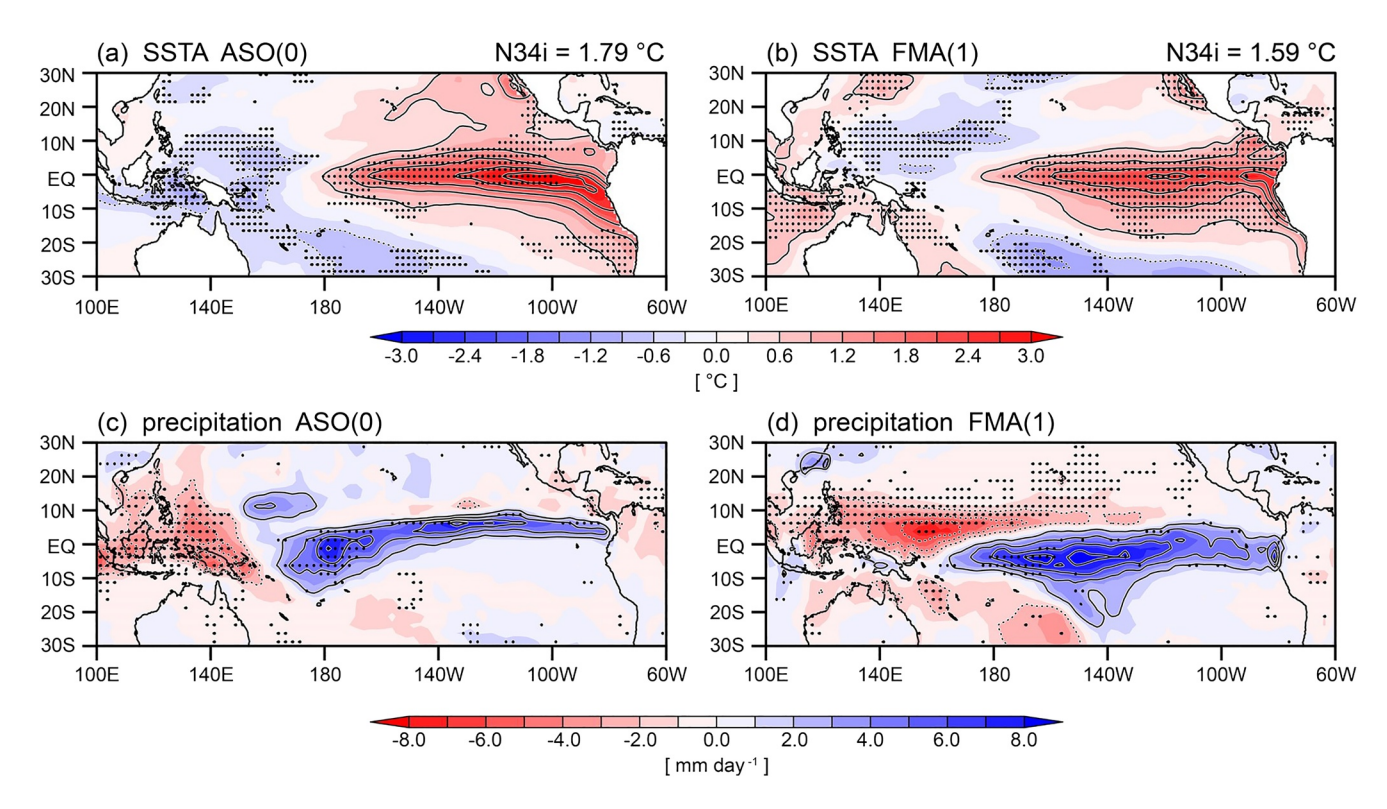


**Figure 1.** Composite anomalies of (a, b) sea surface temperature (SST) and (c, d) precipitation in ASO(0) and FMA(1) in extreme El Niño years, respectively. The contour interval is 0.6°C for SST anomalies and 2 mm day<sup>-1</sup> for precipitation anomalies, with the zero contour omitted. Dots indicate anomalies significant at the 95% confidence level. Numbers on the top right of (a and b) show the composite of Niño3.4 index for each season.

The PC time series show that EOF1 has positive peaks in El Niño years, consistent with the spatial structure and a high correlation with the Niño3.4 index (r = 0.83) (Figure 2c). Interestingly, the PC2 time series is apparently unrelated to ENSO as it contains high-frequency fluctuations unlike the slow ENSO cycle. However, positive peaks are observed immediately after the peak of extreme El Niño events in 1982/83 and 1997/98, preceding negative peaks (Figure 2c). While the PC2 time series is only weakly correlated with the Niño3.4 index (r = 0.28), the time evolution suggests a relationship with extreme El Niño. Hereafter, we refer the precipitation variability represented by EOF2 to as the Pacific precipitation dipole mode (PPDM). There is no clear phase reversal of PPDM in FMA(1) during the most recent extreme event (2015/16), which is explained in reference to the mechanism (Section 3.2).

The EOF analysis was also performed to the 100-member d4PDF ensemble data to examine whether the two leading EOFs are reproduced in the AGCM driven by historical records of SST and sea-ice concentration. Figure S4 shows the results of the EOF analysis for the entire ensemble (100 members concatenated), which reveals that the two leading modes of variability can well be reproduced in terms of both the spatial structure and temporal evolution. The ensemble-mean PC time series (black curves in Figures S4c and S4d) are highly correlated with the observed PC time series (r = 0.91 for EOF1 and r = 0.80 for EOF2). This indicates that the observed dominant modes of precipitation variability have been forced by SST anomalies. The correlation between d4PDF and GPCP is slightly low for PC2, which shows that the ensemble spread is larger than that of PC1, suggesting that the EOF2 partly represents the precipitation variability independent of the underlying SST fluctuations.

To better understand the relationship between the temporal developments of ENSO and the precipitation modes, phase space diagrams are produced from GPCP observations and d4PDF (Figure 3). In this figure, PC1 and PC2 plotted on their phase space are categorized into extreme El Niño (red), moderate El Niño (green), and La Niña (blue) during May(0)-August(1).

The composite mean trajectories in the observations (Figure 3a) clearly show that the temporal evolutions of moderate El Niño and La Niña are symmetric with respect to the climatological mean (i.e., origin). Namely,

FUKUDA ET AL. 4 of 10

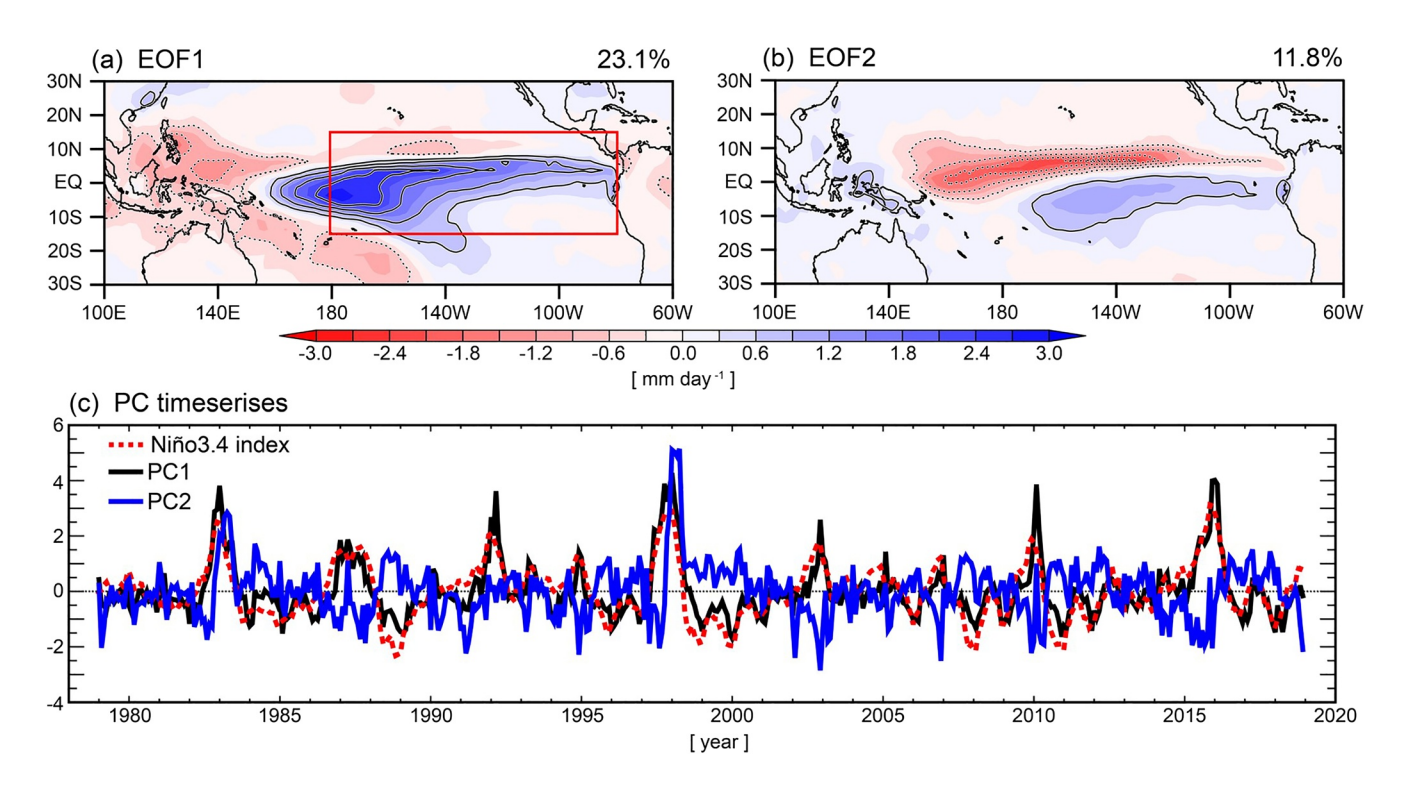


**Figure 2.** (a, b) The two leading modes of tropical Pacific precipitation variability obtained as the first and second empirical orthogonal functions to monthly observed precipitation anomalies from Global Precipitation Climatology Project over the central-eastern equatorial Pacific (red box in (a)). The panels show linear regression of precipitation anomalies on the corresponding principal component (PC) time series shown in (c). The contour interval is 0.6 mm day<sup>-1</sup> and the zero contour is omitted. Numbers on the top right show the fractional variance. In (c), the black and blue solid lines denote PC1 and PC2 time series, respectively, and the Niño3.4 index is denoted by the red dashed line.

EOF1 is positive while EOF2 is negative during moderate El Niño, and vice versa during La Niña. In contrast, the composite trajectory during extreme El Niño shows sign reversal of PC2 from negative in ASO(0) to positive in FMA(1). This phase change corresponds to the increase in precipitation over the northern

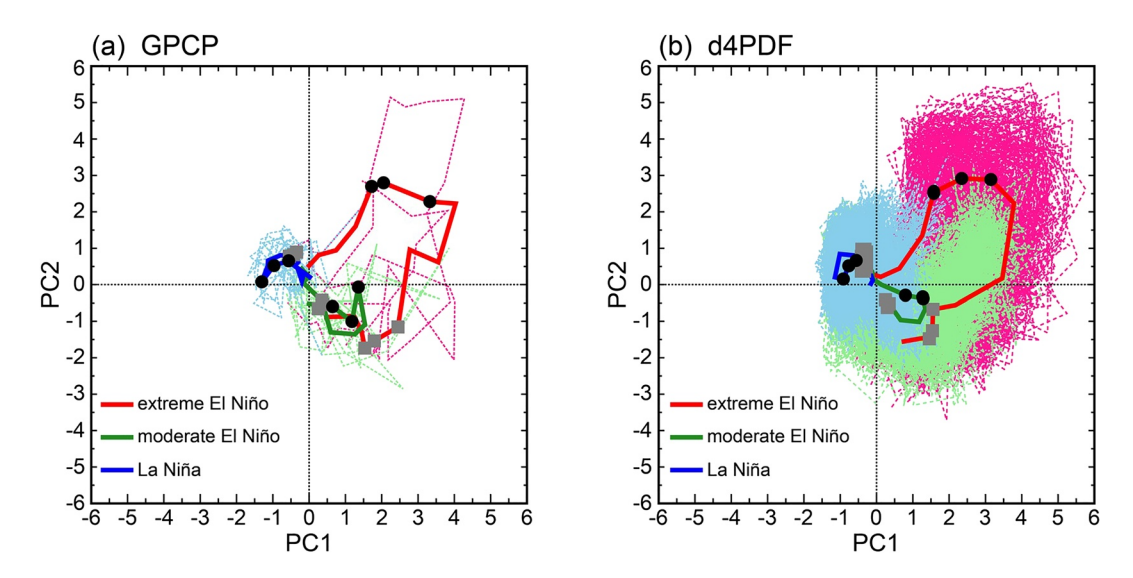


**Figure 3.** Phase space diagrams of the principal component (PC) time series during El Niño/Southern Oscillation events for (a) Global Precipitation Climatology Project and (b) database for Policy Decision making for Future climate change (d4PDF), categorized into extreme El Niño (red), moderate El Niño (green), and La Niña (blue). Thin dashed lines indicate individual events and thick solid lines are their composites. Gray rectangles imposed on the solid lines denote ASO(0) and black circles denote FMA(1). All trajectories evolve counterclockwise.

FUKUDA ET AL. 5 of 10



off-equator during the developing phase of extreme El Niño and over the southern off-equator during the decaying phase. The differences among extreme El Niño, moderate El Niño, and La Niña are clearer in the d4PDF, which has 100-times as large samples as observations, although the trajectories in each category show a certain spread (Figure 3b).

The above analyses show that the distinctive patterns of anomalous precipitation between ASO(0) and FMA(1) in extreme El Niño years can be explained by the phase reversal of the PPDM. The time evolution of the PPDM is linked to the ENSO cycle in a nonlinear fashion as it is amplified only during extreme El Niño. Therefore, the relationship could not be identified by a linear correlation with the Niño3.4 index (Figure 2c).

#### 3.2. Mechanism of PPDM

Given that the PPDM changes its sign before and after the peak of extreme El Niño when the SST anomaly patterns are similar (Figure 1), the excitation of the PPDM cannot be explained solely by the ENSO-induced SST anomalies. The other factor that might be responsible for generating the PPDM is the background mean states of the atmosphere and ocean. Therefore, we examined the differences in precipitation response to a prescribed pattern of SST anomalies under seasonally varying mean states. For this purpose, we conducted mLBM experiments to obtain a steady linear response of moist atmosphere to a prescribed SST anomaly pattern derived from the observed composite of extreme El Niño over the tropical Pacific (Figures 1a and 1b). Using two basic states from the climatological mean fields for ASO and FMA, we calculated the steady response to the identical SST forcing obtained by the average of composite SST anomaly patterns in ASO(0) and FMA(1) during extreme El Niño.

The steady precipitation responses to the prescribed SST anomaly pattern in the mLBM are presented in Figures 4a and 4b. For the ASO basic state, a positive precipitation response is seen in the northern off-equatorial Pacific and a negative response over the western Pacific, similar to the observed composite (Figures 1c and 4a). Likewise, for the FMA basic state, the steady precipitation response broadly reproduces the observed composite, showing a positive precipitation response over the central-eastern Pacific between the equator and 10°S and a negative response over the northwestern equatorial Pacific (Figures 1d and 4b). Differences in the precipitation response in mLBM could be due to different basic states by definition. Thus, the results provide evidence that observed precipitation anomaly patterns in ASO(0) and FMA(1) associated with extreme El Niño occur via a coupling between the SST anomaly pattern and a background seasonal cycle.

The climatological mean SST and convective available potential energy (CAPE) in ASO and FMA are shown in Figures 4c and 4d. It is well known that the atmosphere becomes convectively unstable (measured by CAPE > 500 J kg<sup>-1</sup>) where the underlying SST exceeds a threshold of approximately 27°C. As precipitation anomalies do not occur over regions with a stable atmosphere, the steady precipitation response in the two seasons is anchored to the region where the mean SST is sufficiently high. The equatorial cold tongue with SST below 23°C in the southeastern Pacific is present throughout the year except in FMA, when SST increases and a large CAPE extends from the northern to the southern off-equator (Figure 4d). During this season, the warm pool also expands eastward. Overall, the mean distribution of SST and CAPE in FMA favors the precipitation response to SST anomalies during extreme El Niño (contours imposed in Figures 4c and 4d) to occur over the central-eastern Pacific to the south of the equator (Figure 4b). Similarly, the western Pacific warm pool moves northward in ASO, leading to the precipitation response to the El Niño SST anomaly over the northwestern equatorial Pacific, which is not observed in FMA (Figure 4a).

In summary, the seasonally migrating climatological mean SST, prominent in the eastern equatorial Pacific, can cause the opposite phase of the PPDM to occur even in response to a similar pattern of SST anomalies associated with extreme El Niño. This mechanism explains why PPDM does not change the polarity (from negative to positive) during the 2015/16 extreme El Niño event when the maximum SST anomaly in FMA(1) appears in the central equatorial Pacific, unlike the other two extreme events (Figure S5).

FUKUDA ET AL. 6 of 10



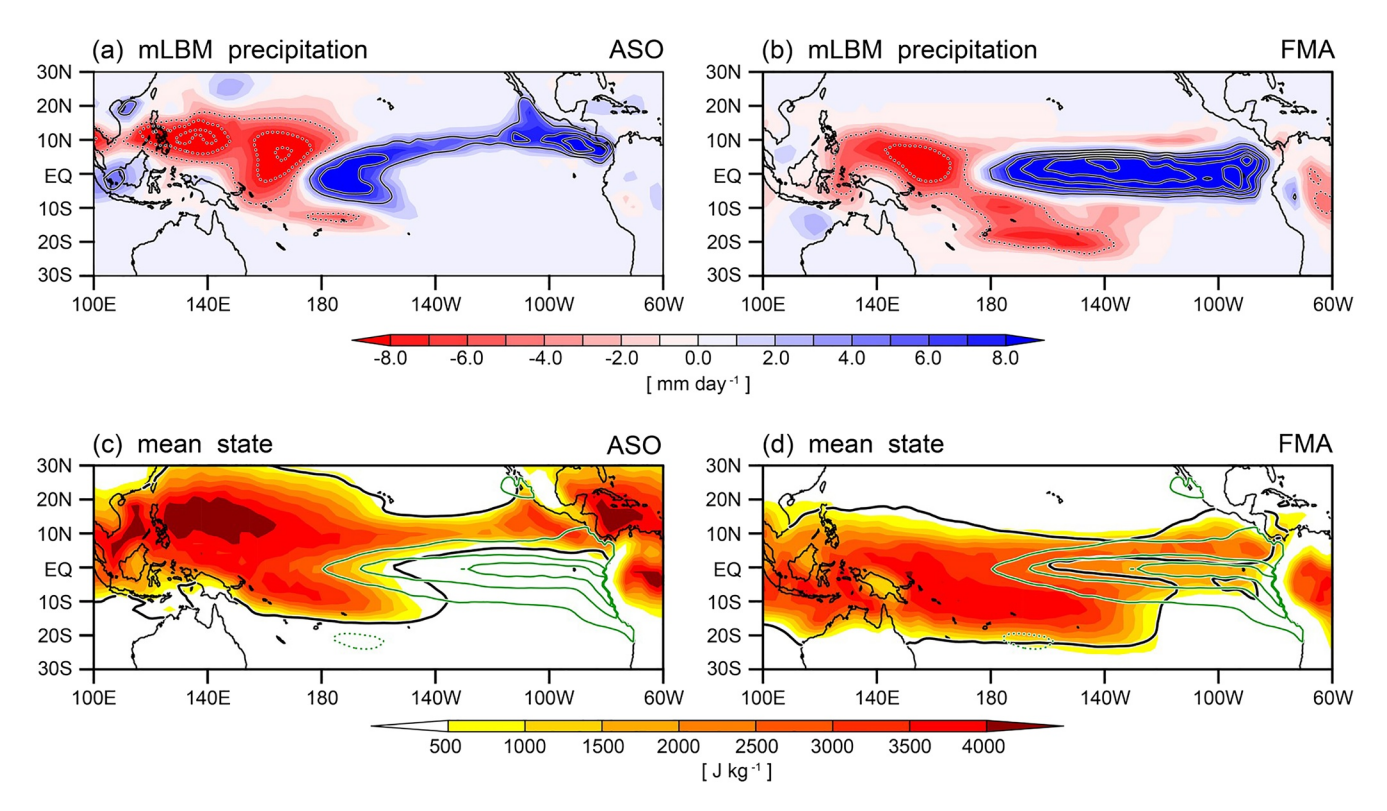


**Figure 4.** (a, b) Steady linear precipitation response to the sea surface temperature (SST) anomaly pattern of extreme El Niño obtained from the moist linear baroclinic model experiments adopting the (a) August-September-October (ASO) and (b) February-March-April (FMA) basic states. The SST anomaly pattern is derived from observed composites during extreme El Niño. The contour interval is 4 mm day $^{-1}$ . (c, d) Climatological mean SST (black contour for 27 $^{\circ}$ C) and convective available potential energy (CAPE) (shading), and the SST forcing pattern (green contour) in (c) ASO and (d) FMA. Region where CAPE is below 500 J kg $^{-1}$  is not shaded. The green contour interval is 0.8 $^{\circ}$ C and the zero contour is omitted.

# 3.3. Relationship With the C-Mode

The ENSO C-mode, defined by the second EOF to the surface zonal wind anomalies over the equatorial Pacific, represents a zonal dipole of the atmospheric circulation pattern at the surface over the western-central Pacific (Figure S6) that is excited by the ENSO-seasonal cycle coupling in the equatorial Pacific (Stuecker, Jin, & Timmermann, 2015; Stuecker, Jin, Timmermann, & Megregon, 2015; Stuecker et al., 2013). Similarities between PPDM and the C-mode, such as phase reversal around extreme El Niño events and the importance of the seasonal cycle coupled to ENSO SST anomalies for the excitation, remind that they represent different aspects of the same phenomenon. Indeed, their PC time series are significantly correlated (r = 0.58), leading to a close resemblance between PPDM and precipitation anomalies regressed on the surface wind EOF2 (C-mode) as well as the C-mode and surface wind anomalies regressed on the precipitation EOF2 (PPDM) (Figure S7, see also Figure S1 of Stuecker, Jin, Timmermann, and Megregon, 2015). An important feature of the C-mode, which has spectral power peaks at combination frequencies of ENSO and the annual cycle, is also confirmed in the PPDM index (Figure S8).

Thus, PPDM is likely a part of the ENSO combination tone and represents a different aspect of the C-mode that has been revealed by the surface wind variability. The correlation between the two time series will be higher if short-term noise unrelated with the ENSO-seasonal cycle coupling is removed. When the PPDM is amplified during extreme El Niño events, the associated diabatic heating is able to force a surface wind response over the western Pacific similar to that of the C-mode (Figure S9), which is not surprising given the tight coupling between circulation and diabatic heating in the tropical atmosphere. In other words, the representation of the ENSO combination tone, that is, a mode arising from the interaction between ENSO and the seasonal cycle, is still an open question, and this study suggests that PPDM is an important component of the extended concept of the ENSO C-mode.

FUKUDA ET AL. 7 of 10



#### 3.4. Impact of PPDM on the Teleconnection

Different precipitation anomaly patterns between extreme and moderate El Niño events during the decay season of FMA(1), mostly due to PPDM, could have a different impact on the East Asian climate via atmospheric teleconnections. For extreme El Niño, positive temperature anomalies in the lower troposphere are significant, whereas such signals are weak for moderate El Niño (Figure S10). The warm condition over East Asia is attributed to the negative precipitation anomaly over the northwestern equatorial Pacific, a part of the PPDM, which can force the low-level anticyclonic circulation anomaly around the Philippines. This anomalous anticyclone accompanying clockwise circulation anomalies would accompany warm air advection from the tropics to the extratropics, causing anomalous warm temperature over East Asia in spring after extreme El Niño (Figure S11). The difference in the impact of extreme and moderate El Niño events on temperature over Japan is identified only in FMA(1) (Figure S12). Although the reason is unclear, this indicates that the different climatic impacts between extreme and moderate El Niño events arise from the difference in the precipitation anomaly patterns but not due to the difference in their magnitude.

# 4. Summary and Discussion

In this study, we investigated the mechanisms of ENSO-seasonal cycle coupling in relevance to precipitation variability over the tropical Pacific. Motivated by the fact that the observed patterns of precipitation anomalies are distinct between autumn before the peak of extreme El Niño and spring after the peak, despite similar patterns of SST anomalies (Figure 1), we examined the leading modes of variability in monthly precipitation from observations and the d4PDF large ensemble.

We identified two leading modes of precipitation variability over the central-eastern Pacific (Figure 2): a zonal dipole pattern obtained as EOF1, representing a typical precipitation anomaly during the mature phase of ENSO, and a meridional dipole pattern obtained as EOF2, which has not been documented to date and termed as the PPDM. The time series of EOF1 is highly correlated with ENSO, whereas PPDM shows only a weak correlation. However, a careful analysis of the time evolution in the phase space reveals a systematic linkage between the PPDM and ENSO (Figure 3). Namely, PPDM changes its sign from negative to positive after the peak of extreme El Niño but retains its sign during moderate El Niño or La Niña. This phase reversal of the PPDM explains the observed seasonally varying precipitation patterns during extreme El Niño.

The mechanism of PPDM was examined using mLBM, which enabled us to obtain a steady moist atmospheric response (including precipitation) to an imposed pattern of SST anomalies as forcings. The model reproduces the precipitation anomaly patterns during extreme El Niño when the observed SST anomaly pattern was given. It was shown that the precipitation response can be different even with the same SST forcing, depending solely on the difference in the basic state taken from autumn and spring climatological states, indicating that the PPDM is excited by a coupling between ENSO and the background seasonal cycle. Specifically, seasonal differences in the mean SST and CAPE over the eastern Pacific are the key as they favor an increase in precipitation over the northern off-equator in autumn, but over the southern off-equator in spring, anchored by the migration of high SST bands (Figure 4).

There may be a feedback of the PPDM to ENSO itself, as expected from a linkage with the C-mode. The linear regression pattern of SST anomalies against the PC2 time series is characterized by negative anomalies in the central equatorial Pacific, accompanied by a southward shift of the equatorial easterly anomalies (Figure S13). The pattern of surface wind anomalies has been reported to damp positive SST anomalies in the central-eastern Pacific by modulating the equatorial thermocline depth (McGregor et al., 2012; Stuecker, Jin, & Timmermann, 2015; Stuecker, Jin, Timmermann, & Megregon, 2015; Stuecker et al., 2013; Vecchi & Harrison, 2003). The phase relationship between the PPDM and the Niño3.4 indices supports the presence of this feedback (Figure S14). Thus, PPDM might contribute to the rapid termination of extreme El Niño, suggesting that PPDM is not a passive response to extreme El Niño but is a part of its nonlinear life cycle.

We have not fully discussed the reason for the selective excitation of the PPDM during extreme El Niño events. There are two apparent differences between extreme and moderate El Niños: amplitudes and longitudes of the maximum SST anomaly. It is plausible that the latter is important as the coupling with the SST

FUKUDA ET AL. 8 of 10



seasonal cycle is relevant in the eastern basin, where moderate El Niño does not have large SST anomalies and therefore is not able to excite PPDM. To fully clarify the role of PPDM in the complex ENSO cycle, we need further analyses and numerical experiments, which will be the subject of future studies.

# **Data Availability Statement**

The observational SST and precipitation data, COBE-SST2 and GPCP, are available at https://psl.noaa.gov/data/gridded/data.cobe2.html and https://psl.noaa.gov/data/gridded/data.gpcp.html. The JRA-55 reanal-ysis data can be downloaded from multiple sites (https://jra.kishou.go.jp/JRA-55/index\_en.html#jra-55). The full d4PDF large ensemble data are stored and available in the Data Integration and Analysis System (https://diasjp.net/en/service/d4pdf-data-download/). The linear baroclinic model used in this study is available at https://ccsr.aori.u-tokyo.ac.jp/~lbm/sub/lbm.html.

#### Acknowledgments

We acknowledge the modeling group for making the d4PDF data set available. We thank Yu Kosaka and the two anonymous reviewers for their constructive comments. This work was supported by the Grant-in-Aid 26247079 and the Integrated Research Program for Advancing Climate Models (TOUGOU) grant number JPMXD0717935457 from the Ministry of Education, Culture, Sports, Science and Technology (MEXT), Japan.

#### References

- Adler, R. F., Huffman, G. J., Chang, A., Ferraro, R., Xie, P.-P., Janowiak, J., et al. (2003). The version-2 global precipitation climatology project (GPCP) monthly precipitation analysis (1979–present). *Journal of Hydrometeorology*, 4, 1147–1167. https://doi.org/10.1175/1525-7541(2003)004<1147:TVGPCP>2.0.CO;2
- Borlace, S., Santoso, A., Cai, W., & Collins, M. (2014). Extreme swings of the South Pacific convergence zone and the different types of El Niño events. *Geophysical Research Letters*, 41, 4695–4703. https://doi.org/10.1002/2014GL060551
- Cai, W., Lengaigne, M., Borlace, S., Collins, M., Cowan, T., McPhaden, M. J., et al. (2012). More extreme swings of the South Pacific convergence zone due to greenhouse warming. *Nature*, 488, 365–369. https://doi.org/10.1038/nature11358
- Chiodi, A. M., & Harrison, D. E. (2013). El Niño impacts on seasonal U.S. atmospheric circulation, temperature, and precipitation anomalies: The OLR-event perspective. *Journal of Climate*, 26, 822–837. https://doi.org/10.1175/JCLI-D-12-00097.1
- Choi, K. Y., Vecchi, G. A., & Wittenberg, A. T. (2013). ENSO transition, duration, and amplitude asymmetries: Role of the nonlinear wind stress coupling in a conceptual model. *Journal of Climate*, 26, 9462–9476. https://doi.org/10.1175/JCLI-D-13-00045.1
- Choi, K. Y., Vecchi, G. A., & Wittenberg, A. T. (2015). Nonlinear zonal wind response to ENSO in the CMIP5 models: Roles of the zonal and meridional shift of the ITCZ/SPCZ and the simulated climatological precipitation. *Journal of Climate*, 28, 8556–8573. https://doi.org/10.1175/JCLI-D-15-0211.1
- Hirahara, S., Ishii, M., & Fukuda, Y. (2014). Centennial-scale sea surface temperature analysis and its uncertainty. *Journal of Climate*, 27, 57–75. https://doi.org/10.1175/JCLI-D-12-00837.1
- Hoerling, M. P., Kumar, A., & Xu, T. (2001). Robustness of the nonlinear climate response to ENSO's extreme phases. *Journal of Climate*, 14, 1277–1293. https://doi.org/10.1175/1520-0442(2001)014<1277:ROTNCR>2.0.CO;2
- Horel, J. D., & Wallace, J. M. (1981). Planetary-scale atmospheric phenomena associated with the Southern Oscillation. *Monthly Weather Review*, 109, 813–829. https://doi.org/10.1175/1520-0493(1981)109<0813:PSAPAW>2.0.CO;2
- Hoskins, B. J., & Karoly, D. J. (1981). The steady linear response of a spherical atmosphere to thermal and orographic forcing. *Journal of the Atmospheric Sciences*, 38, 1179–1196. https://doi.org/10.1175/1520-0469(1981)038<1179:TSLROA>2.0.CO;2
- Jin, F. F., Neelin, J. D., & Ghil, M. (1994). El Niño on the devil's staircase: Annual subharmonic steps to chaos. Science, 264, 70–72. https://doi.org/10.1126/science.264.5155.70
- Johnson, N. C., & Kosaka, Y. (2016). The impact of eastern equatorial Pacific convection on the diversity of boreal winter El Niño teleconnection patterns. Climate Dynamics, 47, 3737–3765. https://doi.org/10.1007/s00382-016-3039-1
- Kobayashi, S., Ota, Y., Harada, Y., Ebita, A., Moriya, M., Onoda, H., et al. (2015). The JRA-55 reanalysis: General specifications and basic characteristics. *Journal of the Meteorological Society of Japan*, 93, 5–48. https://doi.org/10.2151/jmsj.2015-001
- McGregor, S., Timmermann, A., Schneider, N., Stuecker, M. F., England, M. H., McGregor, S., et al. (2012). The effect of the South Pacific convergence zone on the termination of El Niño events and the meridional asymmetry of ENSO. *Journal of Climate*, 25, 5566–5586. https://doi.org/10.1175/JCLI-D-11-00332.1
- Mizuta, R., Murata, A., Ishii, M., Shiogama, H., Hibino, K., Mori, N., et al. (2017). Over 5,000 years of ensemble future climate simulations by 60-km global and 20-km regional atmospheric models. *The Bulletin of the American Meteorological Society*, 98, 1383–1398. https://doi.org/10.1175/BAMS-D-16-0099.1
- Neelin, J. D., Battisti, D. S., Hirst, A. C., Jin, F.-F., Wakata, Y., Yamagata, T., & Zebiak, S. E. (1998). ENSO theory. *Journal of Geophysical Research*, 103, 14261–14290. https://doi.org/10.1029/97JC03424
- Okumura, Y. M. (2019). ENSO diversity from an atmospheric perspective. Current Climate Change Reports, 5, 245–257. https://doi.org/10.1007/s40641-019-00138-7
- Spencer, H. (2004). Role of the atmosphere in seasonal phase locking of El Niño. Geophysical Research Letters, 31, L24104. https://doi.org/10.1029/2004GL021619
- Stein, K., Timmermann, A., Schneider, N., Jin, F.-F., Stuecker, M. F., Stein, K., et al. (2014). ENSO seasonal synchronization theory. *Journal of Climate*, 27, 5285–5310. https://doi.org/10.1175/JCLI-D-13-00525.1
- Stuecker, M. F., Jin, F. F., & Timmermann, A. (2015). El Niño—Southern Oscillation frequency cascade. *Proceedings of the National Academy of Sciences of the United States of America*, 112, 13490–13495. https://doi.org/10.1073/pnas.1508622112
- Stuecker, M. F., Jin, F. F., Timmermann, A., & Mcgregor, S. (2015). Combination mode dynamics of the anomalous northwest pacific anticyclone. *Journal of Climate*, 28, 1093–1111. https://doi.org/10.1175/JCLI-D-14-00225.1
- Stuecker, M. F., Timmermann, A., Jin, F.-F., McGregor, S., & Ren, H.-L. (2013). A combination mode of the annual cycle and the El Niño/Southern Oscillation. *Nature Geoscience*, 6, 540–544. https://doi.org/10.1038/ngeo1826
- Tziperman, E., Stone, L., Cane, M. A., & Jarosh, H. (1994). El Niño chaos: Overlapping of resonances between the seasonal cycle and the pacific ocean-atmosphere oscillator. *Science*, 264, 72–74. https://doi.org/10.1126/science.264.5155.72
- Vecchi, G. A., & Harrison, D. E. (2003). On the termination of the 2002–03 El Niño event. Geophysical Research Letters, 30(18), 1964. https://doi.org/10.1029/2003GL017564

FUKUDA ET AL. 9 of 10



10.1029/2021GL095204



- Wallace, J. M., Rasmusson, E. M., Mitchell, T. P., Kousky, V. E., Sarachik, E. S., & Von Storch, H. (1998). On the structure and evolution of ENSO-related climate variability in the tropical Pacific: Lessons from TOGA. *Journal of Geophysical Research*, 103, 14241–14259. https://doi.org/10.1029/97JC02905
- $Watanabe, M., \& Jin, F.-F. (2003). A moist linear baroclinic model: Coupled dynamical-convective response to El Niño. \textit{Journal of Climate, } 16, 1121-1139. \\ \text{https://doi.org/10.1175/1520-0442(2003)16<1121:AMLBMC>2.0.CO;2}$
- Xie, S.-P., Peng, Q., Kamae, Y., Zheng, X.-T., Tokinaga, H., Wang, D., et al. (2018). Eastern Pacific ITCZ dipole and ENSO diversity. *Journal of Climate*, 31, 4449–4462. https://doi.org/10.1175/JCLI-D-17-0905.1
- Yu, J. Y., Zou, Y., Kim, S. T., & Lee, T. (2012). The changing impact of El Niño on US winter temperatures. *Geophysical Research Letters*, 39, L15702. https://doi.org/10.1029/2012GL052483
- Yuan, Y., & Yang, S. (2012). Impacts of different types of El Niño on the East Asian climate: Focus on ENSO cycles. *Journal of Climate*, 25, 7702–7722. https://doi.org/10.1175/JCLI-D-11-00576.1
- Zebiak, S. E., Cane, M. A., Zebiak, S. E., & Cane, M. A. (1987). A model El Niño–Southern Oscillation. *Monthly Weather Review*, 115, 2262-2278. https://doi.org/10.1175/1520-0493(1987)115<2262:AMENO>2.0.CO;2

FUKUDA ET AL. 10 of 10